Site-Specific Nitration and Oxidative Dityrosine Bridging of the τ Protein by Peroxynitrite: Implications for Alzheimer's Disease †

ARTICLE *in* BIOCHEMISTRY · FEBRUARY 2005

Impact Factor: 3.02 · DOI: 10.1021/bi047982v · Source: PubMed

3 AUTHORS, INCLUDING:

Lester I Binder
Michigan State University
144 PUBLICATIONS **14,074** CITATIONS

SEE PROFILE

Site-Specific Nitration and Oxidative Dityrosine Bridging of the τ Protein by Peroxynitrite: Implications for Alzheimer's Disease†

Matthew R. Reynolds,*,‡ Robert W. Berry,‡,§ and Lester I. Binder‡,§

Department of Cell and Molecular Biology and Cognitive Neurology and Alzheimer's Disease Center, Feinberg School of Medicine, Northwestern University, Chicago, Illinois 60611

Received September 19, 2004; Revised Manuscript Received November 4, 2004

ABSTRACT: Alzheimer's disease (AD) is a progressive amnestic disorder typified by the pathological misfolding and deposition of the microtubule-associated τ protein into neurofibrillary tangles (NFTs). While numerous post-translational modifications influence NFT formation, the molecular mechanisms responsible for τ aggregation remain enigmatic. Since nitrative and oxidative injury have previously been shown to play a mechanistic role in neurodegeneration, we examined whether these events influence τ aggregation. In this report, we characterize the effects of peroxynitrite ($ONOO^-$)-mediated nitration and oxidation on τ polymerization *in vitro*. Treatment of τ with $ONOO^-$ results in 3-nitrotyrosine (3-NT) immunoreactivity and the formation of heat-stable, SDS-insoluble oligomers. Using ESI-MS and HPLC with fluorescent detection, we show that these higher-order aggregates contain 3,3′-dityrosine (3,3′-DT). Tyrosine (Tyr) residues are critical for $ONOO^-$-mediated oligomerization, as τ proteins lacking all Tyr residues fail to generate oligomers upon $ONOO^-$ treatment. Further, τ nitration targets residues Y18, Y29, and to a lesser degree Y197 and Y394, and nitration at these sites inhibits *in vitro* polymerization. The inhibitory effect of nitration on τ polymerization is specific for the 3-NT modification, as pseudophosphorylation at these same Tyr residues does not inhibit τ assembly. Our results suggest that the nitrative and oxidative roles of $ONOO^-$ differentially affect τ polymerization and that $ONOO^-$-mediated cross-linking could facilitate τ aggregation in AD.

Alzheimer's disease (AD)[1] is a progressive neurodegenerative disorder characterized by the pathological self-assembly of the microtubule-associated τ protein into neurofibrillary tangles (NFTs). In solution, τ is a natively unfolded protein dominated by random coil structure (*1*). In AD brain, however, aberrant modifications of τ, including phosphorylation, truncation, and conformational changes, induce polymer formation (*2*−*6*) by causing certain regions of the molecule to adopt a β-pleated sheet conformation (*7*−*9*). Therefore, to fully understand the mechanisms that govern τ misfolding, we must first delineate the modifications that drive and/or stabilize τ polymerization.

Nitrative and oxidative injury are salient features of AD-associated inflammation (*10*−*13*). During this process, reactive nitrogen and oxygen species are generated that can modify protein tyrosine (Tyr) residues (*14*). Principal among these species is peroxynitrite ($ONOO^-$), a powerful *in vivo* oxidant capable of protein nitration and oxidation (*15*). $ONOO^-$ is generated from the near-diffusion-limited reaction of nitric oxide ($NO^\bullet$) and superoxide ($O_2^{\bullet-}$) radicals (*16*). Reaction of $ONOO^-$ with proteins can lead to the addition of a nitro (NO_2) group onto the *ortho* carbon of the Tyr ring to yield 3-nitrotyrosine (3-NT). Moreover, $ONOO^-$ is able to cross-link proteins by the oxidative addition of two tyrosyl radicals to form 3,3′-dityrosine (3,3′-DT) (*17*, *18*).

3-NT and 3,3′-DT levels are significantly elevated in AD hippocampus (*19*), and 3-NT-modified proteins selectively localize to NFTs in post-mortem AD brain (*10*, *11*). Using antibodies specific to nitrated α-synuclein, Giasson and colleagues show robust staining of the signature protein aggregates in Parkinson's disease (*20*). Similarly, immunological probes raised against nitrated α-synuclein that also recognize nitrated τ decorate NFTs and τ inclusions in AD brain (*21*). More recent work demonstrates that $ONOO^-$ can induce α-synuclein oligomerization through covalent 3,3′-DT cross-linking (*17*). Taken together, these data suggest that $ONOO^-$ may facilitate the misfolding and deposition of select proteins through nitrative and/or oxidative modification.

Here we report that τ is a substrate for nitration and oxidation by $ONOO^-$ *in vitro*, leading to the formation of covalently coupled, SDS-resistant oligomers. While the oxidative role of $ONOO^-$ promotes oligomerization via 3,3′-

† This work was supported in part by NIH Grants AG14453 and AG21184.

* To whom correspondence should be addressed: Feinberg School of Medicine, Northwestern University, Tarry Building 8-754, 303 E. Chicago Ave., Chicago, IL 60611. Phone: (312) 503-0824. Fax: (312) 503-7912. E-mail: m-reynolds@md.northwestern.edu.

‡ Department of Cell and Molecular Biology, Northwestern University.

§ Cognitive Neurology and Alzheimer's Disease Center, Northwestern University.

[1] Abbreviations: AD, Alzheimer's disease; EM, electron microscopy; 3,3′-DT, 3,3′-dityrosine; ESI-MS, electrospray ionization mass spectrometry; HPLC, high-performance liquid chromatography; LLS, right-angle laser light scattering; MALDI-TOF MS, matrix-assisted laser desorption ionization time-of-flight mass spectrometry; MPO, myeloperoxidase; NFT, neurofibrillary tangle; 3-NT, 3-nitrotyrosine; $ONOO^-$, peroxynitrite; SDS−PAGE, sodium dodecyl sulfate−polyacrylamide gel electrophoresis.

10.1021/bi047982v CCC: $30.25
Published on Web 01/13/2005

Table 1: Nomenclature and Description of All hτ40 Mutants Used in This Study[a]

Nomenclature	Description	Purpose
^{18}Y	hτ40 harboring a single Tyr at Tyr18; i.e., $^{Y}29^{F}$, $^{Y}197^{F}$, $^{Y}310^{F}$, $^{Y}394^{F}$	To target Tyr18 for oxidative and/or nitrative modification
^{29}Y	hτ40 harboring a single Tyr at Tyr29; i.e., $^{Y}18^{F}$, $^{Y}197^{F}$, $^{Y}310^{F}$, $^{Y}394^{F}$	To target Tyr29 for oxidative and/or nitrative modification
^{197}Y	hτ40 harboring a single Tyr at Tyr197; i.e., $^{Y}18^{F}$, $^{Y}29^{F}$, $^{Y}310^{F}$, $^{Y}394^{F}$	To target Tyr197 for oxidative and/or nitrative modification
^{310}Y	hτ40 harboring a single Tyr at Tyr310; i.e., $^{Y}18^{F}$, $^{Y}29^{F}$, $^{Y}197^{F}$, $^{Y}394^{F}$	To target Tyr310 for oxidative and/or nitrative modification
^{394}Y	hτ40 harboring a single Tyr at Tyr394; i.e., $^{Y}18^{F}$, $^{Y}29^{F}$, $^{Y}197^{F}$, $^{Y}310^{F}$	To target Tyr394 for oxidative and/or nitrative modification
5x Y → F	hτ40 lacking all Tyr residues; i.e., $^{Y}18^{F}$, $^{Y}29^{F}$, $^{Y}197^{F}$, $^{Y}310^{F}$, $^{Y}394^{F}$	Negative control for Tyr modification
$^{C}291^{A}/^{C}322^{A}$	hτ40 doubly mutated at both Cys residues; i.e., $^{C}291^{A}$ and $^{C}322^{A}$	Negative control for oxidative disulfide bond formation
$^{Y}18^{E}$	hτ40 harboring a single Y → E mutation at Tyr18	To mimic phosphorylation at Tyr18
$^{Y}29^{E}$	hτ40 harboring a single Y → E mutation at Tyr29	To mimic phosphorylation at Tyr29
$^{Y}197^{E}$	hτ40 harboring a single Y → E mutation at Tyr197	To mimic phosphorylation at Tyr197
$^{Y}310^{E}$	hτ40 harboring a single Y → E mutation at Tyr310	To mimic phosphorylation at Tyr310
$^{Y}310^{F}$	hτ40 harboring a single Y → F mutation at Tyr310	To control for the effects of $^{Y}310^{E}$ on hτ40 polymerization
$^{Y}394^{E}$	hτ40 harboring a single Y → E mutation at Tyr394	To mimic phosphorylation at Tyr394

[a] Full-length human τ (hτ40) contains five Tyr residues located at positions 18, 29, 197, 310, and 394.

DT cross-linking, the nitrative role of $ONOO^-$ inhibits τ polymerization. The inhibitory effect of nitration on τ assembly is influenced by the chemical nature of the 3-NT modification, as pseudophosphorylation at these same Tyr residues does not affect τ polymerization.

EXPERIMENTAL PROCEDURES

Mutagenesis, Expression, and Purification of hτ40. The pT7C-hτ40 plasmid that drives the expression of full-length human τ (hτ40) fused to an N-terminal six-His affinity tag has been described previously (*22*). The hτ40 cDNA was mutagenized using a site-directed mutagenesis kit (Stratagene) with primers that define the sequence flanking each targeted codon. In some instances, multiple rounds of mutagenesis were performed to alter two or more amino acids on the hτ40 protein. A summary of the hτ40 mutants used in this study, along with their adopted nomenclature, is presented in Table 1. All mutations were confirmed by DNA sequencing. Wild-type and mutant hτ40 proteins were expressed in BL21 cells (Invitrogen) and purified over a Ni−NTA agarose column (Qiagen) (*23*). Size-exclusion chromatography was also performed to separate full-length hτ40 from C-terminal truncation products and incompletely translated hτ40 proteins that retain the N-terminal affinity tag (*23*). Protein concentrations were determined by the Lowry method using bovine serum albumin as a standard (*24*).

Nitration and/or Oxidation of Wild-Type and Mutant hτ40. $ONOO^-$ was prepared from sodium nitrite and acidified H_2O_2 as described previously (*25*). Unreacted H_2O_2 was removed by passing the $ONOO^-$ stock solution over a manganese dioxide column (*26*). The $ONOO^-$ concentration was measured spectrophotometrically at 302 nm in 0.3 M NaOH (ϵ_{302} = 1670 M^{-1} cm^{-1}) prior to each experiment (*27*). Wild-type and mutant hτ40 proteins (4−6 mg/mL) were buffer exchanged into nitration buffer [100 mM potassium phosphate, 25 mM sodium bicarbonate (pH 7.4), and 0.1 mM diethylenetriaminepentaacetic acid] (*28*) and treated with a 0.5-, 5.0-, 10-, 50-, or 100-fold molar excess of $ONOO^-$. $ONOO^-$ was added as two boluses with vigorous stirring for 30 s at room temperature. The final pH was measured and kept at pH 7.4 (*28*). As a negative control for nitration, $ONOO^-$ was degraded in nitration buffer prior to addition to the hτ40 solution (*29*).

Nitrated wild-type and mutant hτ40 proteins were boiled for 10 min in Laemmli sample buffer [0.125 M Tris (pH 6.8), 4% SDS, 20% glycerol, and 10% β-mercaptoethanol], resolved electrophoretically, and transferred onto nitrocellulose membranes. Membranes were blocked for 1 h in a 5% (w/v) solution of nonfat dry milk and then incubated for 16 h at 4 °C in a polyclonal 3-NT (Chemicon; 1 μg/mL) or monoclonal Tau-5 (20 ng/mL) antibody solution. Following a secondary incubation with a HRP-conjugated anti-mouse or anti-rabbit antibody (Jackson ImmunoResearch), the membranes were developed using enhanced chemiluminescence (Amersham Biosciences) and exposed to autoradiographic film. To validate the specificity of the 3-NT antibody, the 3-NT moiety was chemically reduced to 3-aminotyrosine prior to Western detection by exposing duplicate membranes to 0.5 M sodium hydrosulfite (Sigma) in 0.1 M NaOH under argon (*30*).

As an independent measure of oxidation, wild-type and mutant hτ40 proteins (4−6 mg/mL) were reacted with 0.25 μM human myeloperoxidase (MPO, Calbiochem) and 200 μM H_2O_2 for 1 h at room temperature (*17*). To assay for both nitrative and oxidative conditions, wild-type and mutant hτ40 proteins were treated with 0.25 μM human MPO, 200 μM H_2O_2, and 100 μM $NaNO_2$ as described previously (*17*).

Characterization of 3,3′-Dityrosine. Wild-type hτ40 proteins (30 mg) were extensively dialyzed against nitration buffer and treated with a 100-fold molar excess of $ONOO^-$. The hτ40 oligomers were separated from monomeric, nitrated hτ40 proteins using gel filtration with a high-resolution Sephacryl S-300 matrix (Amersham Biosciences) (*23*). Purified hτ40 oligomers were hydrolyzed into their constituent amino acids by reaction with 6 N HCl at 110 °C for 16 h under argon. The hydrolysates were lyophilized, resuspended into 0.1% trifluoroacetic acid (TFA), and separated on a Platinum C_{18} reverse-phase column (5 μm, 300 Å, 250 mm × 4.6 mm, Alltech) at 1 mL/min. High-performance

liquid chromatography (HPLC) was performed on a HP 1100 system (Hewlett-Packard) using a linear gradient of 0 to 15% acetonitrile containing 0.1% TFA over the course of 30 min. Eluates were monitored by their UV absorbance at 215 nm and their fluorescent emission profile ($\lambda_{ex} = 283$ nm, $\lambda_{em} = 410$ nm). L-Tyrosine, 3,3′-dityrosine, and 3-nitro-L-tyrosine were identified by their coelution with external standards. The 3,3′-dityrosine standard was synthesized by reacting horseradish peroxidase with L-tyrosine and H_2O_2 (*28*).

Electrospray ionization mass spectrometry (ESI-MS) was performed on a 1100 LC/MSD Trap XCT system (Agilent Technologies) equipped with an electrospray source operating in the positive ion mode. Nitrated and nonmodified hτ40 hydrolysates were separated on a Platinum C_{18} reverse-phase column (5 μm, 300 Å, 250 mm × 4.6 mm, Alltech) at a flow rate of 400 μL/min. An increasing linear gradient from 0 to 15% acetonitrile containing 0.1% formic acid was used to resolve the reaction products. The ESI conditions were as follows: capillary temperature of 325 °C, nitrogen sheath gas pressure of 18 psi, and ion spray voltage of 2.5 kV. Tandem MS/MS was also performed using collision-induced dissociation to further characterize the 3,3′-DT product. All mass spectra were externally calibrated.

Mass Mapping of Site-Specific hτ40 Nitration. For peptide mass fingerprinting analysis, 100 pmol of hτ40 treated with a 100-fold molar excess of either degraded or active $ONOO^-$ was digested with sequence-grade trypsin (Promega) for 16 h. Tryptic peptides were dried under vacuum, resuspended in 0.1% TFA, desalted with C_{18} ziptips (Millipore), and eluted onto the MS target plate in a 0.1% TFA/50% acetonitrile mixture saturated with α-cyano-4-hydroxycinnamic acid. Peptides were analyzed using a Voyager DE-Pro matrix-assisted laser desorption ionization time-of-flight (MALDI-TOF) mass spectrometer in the reflector positive ion mode (Perseptive Biosystems). The accelerating voltage was set to 20 000 V, and the grid voltage was 70%. The laser setting varied between 2800 and 3100, and data were acquired using 100 scans/spectrum with an acquisition mass range from 500 to 3500 Da. All mass spectra were externally calibrated.

Cleavage of the N-terminal six-His affinity tag was performed using a Thrombin CleanCleave kit (Sigma) according to the manufacturer's instructions. Briefly, hτ40 proteins (1 mg/mL) were extensively dialyzed against cleavage buffer [50 mM Tris-HCl (pH 8.0) and 10 mM $CaCl_2$] and digested for 1 h at room temperature with thrombin−agarose resin. Following cleavage, the resin was removed via centrifugation (10 000*g*), and cleavage efficiency was assayed by Western blot using anti-six-His (Calbiochem; 1 μg/mL) and Tau-5 (20 ng/mL) antibodies.

In Vitro Polymerization and Electron Microscopy. Wild-type, nitrated, and mutant hτ40 proteins were diluted in polymerization buffer [10 mM HEPES (pH 7.4), 100 mM NaCl, and 5 mM DTT] to a final concentration of 4 μM. Nitrated, monomeric hτ40 was isolated via size-exclusion chromatography as described in detail above. Polymerization was induced with arachidonic acid (75 μM), and right-angle laser light scatter (LLS) was monitored over a 6 h period (*31*). It was previously demonstrated that the N-terminal six-His affinity tag has no effect on *in vitro* hτ40 assembly (*32*). All data were fit by nonlinear regression to one- or two-phase exponential association curves.

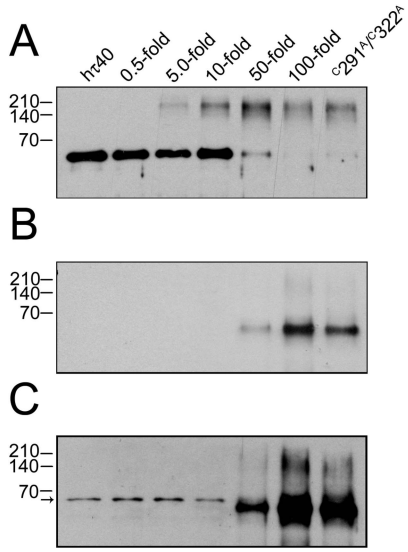

FIGURE 1: Treatment of hτ40 with $ONOO^-$ induces 3-NT immunoreactivity and the formation of heat-stable, SDS-resistant oligomers. Full-length τ (hτ40) protein was treated with a 0.5-, 5.0-, 10-, 50-, or 100-fold molar excess of $ONOO^-$, fractionated by SDS−PAGE, transferred onto nitrocellulose membranes, and detected using the antibodies Tau-5 (A) and 3-NT (B and C). Panel C illustrates a longer exposure time of the blot from panel B. As a negative control, hτ40 was treated with degraded $ONOO^-$ (lane 1). hτ40 doubly mutated at both cysteine residues ($^C291^A/^C322^A$) was also treated with a 100-fold molar excess of $ONOO^-$ and processed alongside hτ40 proteins. The band migrating at 69 kDa (C, arrow) can be attributed to cross-reactivity of the 3-NT antibody with unmodified hτ40. Five (A) and fifty (B and C) nanograms of protein were loaded per well. Results are representative of four independent experiments.

After 6 h, polymerization samples were fixed in 2% (w/v) glutaraldehyde for electron microscopy (EM) analysis. 300-mesh, carbon-coated Formvar grids (Electron Microscopy Sciences) were prepared and negatively stained using 2% (w/v) uranyl acetate (*31*). Grids were analyzed using the JEOL JEM-1220 EM instrument at 60 kV and a magnification of 20 000×. For each sample, grids were prepared in duplicate and filament dimensions were quantified from six random images per grid (*32*). Images were processed in Adobe Photoshop 7.0, and quantification was performed using Optimas 6.5 software (Media Cybernetics) as described previously (*32*). The average mass of filaments per field was determined by multiplying the field's average filament length by the average filament number. The level of statistical significance was set at 0.05 (two-tailed *t* test).

RESULTS

$ONOO^-$ Induces the Nitration and SDS-Resistant Oligomerization of hτ40. To examine the effects of nitrative and oxidative injury on τ aggregation, full-length human τ (hτ40) protein was treated with increasing molar equivalents of $ONOO^-$. Nitration and total τ protein were assayed by Western blot using 3-NT and Tau-5 antibodies, respectively. As shown by SDS−PAGE, the level of monomeric hτ40 (68 kDa) decreases as a function of increasing $ONOO^-$ concentration (Figure 1A). This reduction of Tau-5 immunoreactivity at 68 kDa can be attributed to the loss of monomeric hτ40 and not to artifactual loss of antibody binding, as confirmed by Coomassie blue staining and immunodetection with a panel of τ antibodies that span the

length of the molecule (data not shown). Moreover, the decrease in the level of monomeric hτ40 coincides with the appearance of heat-stable, SDS-insoluble oligomers ranging in size from 140 (dimer) to 210 kDa (trimer). It is noteworthy to include that the decrease in the level of hτ40 monomer does not appear to be proportional to the increase in the level of hτ40 oligomers, as would be predicted by densitometry analysis. This observation can be explained by the fact that Western blot transfer efficiencies are inversely proportional to protein size, especially for proteins larger than 100 kDa. In fact, by Coomassie blue staining, we observed incomplete transfer of high-molecular mass hτ40 oligomers from the gel to the membrane (data not shown). While substoichiometric amounts of $ONOO^-$ fail to induce hτ40 oligomerization, concentrations of ≥5-fold efficiently aggregate hτ40 proteins. Formation of disulfide bonds is not required for $ONOO^-$-mediated oligomerization, as hτ40 lacking both cysteine residues ($^{C}291^{A}/^{C}322^{A}$) also produces high-molecular mass aggregates (Figure 1A).

$ONOO^-$ also induces monomeric hτ40 nitration at a ≥50-fold molar excess (Figure 1B). These bands are specific to the 3-NT modification, as reduction of the 3-NT group to 3-aminotyrosine with sodium hydrosulfite abolishes this immunoreactivity (data not shown). The 3-NT antibody also detects doubly mutated hτ40 ($^{C}291^{A}/^{C}322^{A}$), suggesting that nitrated sulfhydryl groups are not responsible for the 3-NT reactivity. It merits attention that the amount of protein loaded per lane in Figure 1B is 10-fold greater than that loaded in Figure 1A (50 and 5 ng, respectively). For this reason, upon treatment with high $ONOO^-$ concentrations, monomeric hτ40 appears to be completely consumed in Figure 1A, yet its presence is apparent in Figure 1B. Longer exposure times with the 3-NT antibody reveal a high-molecular mass smear ranging from ~140 to 210 kDa (Figure 1C). The additional exposure time needed to visualize the hτ40 oligomers suggests that these aggregates may not be heavily nitrated. A possible explanation for the relative lack of 3-NT in the hτ40 aggregates is that other modifications of Tyr may destabilize the phenolic ring and render it less susceptible to nitration. The protein band migrating at 69 kDa (Figure 1C, arrow) can be attributed to cross-reactivity of the primary antibody with unmodified hτ40.

Oxidation Alone Promotes hτ40 Oligomerization. To delineate whether the oxidative or nitrative role of $ONOO^-$ is responsible for hτ40 oligomerization, we exposed hτ40 to either oxidative [myeloperoxidase (MPO) and H_2O_2] or oxidative and nitrative (MPO, H_2O_2, and NO_2^-) conditions. Treatment of hτ40 with MPO and H_2O_2 results in the formation of higher-order bands at 140 and 210 kDa (Figure 2A). This observation strongly suggests that oxidative conditions alone are sufficient to generate hτ40 aggregates. The combination of MPO, H_2O_2, and NO_2^- synergistically promotes hτ40 oligomerization, as seen from the intense signal around ~140−210 kDa. The formation of disulfide bonds is not entirely responsible for this oxidative cross-linking because a double hτ40 mutant lacking cysteine residues ($^{C}291^{A}/^{C}322^{A}$; designated "Cysless" in Figure 2) is aggregation competent. Interestingly, treatment of the $^{C}291^{A}/^{C}322^{A}$ double mutant with MPO, H_2O_2, and NO_2^- does not significantly enhance aggregation compared to treatment with oxidative conditions alone (Figure 2A, compare lanes 4 and 5). This observation suggests that, under these conditions,

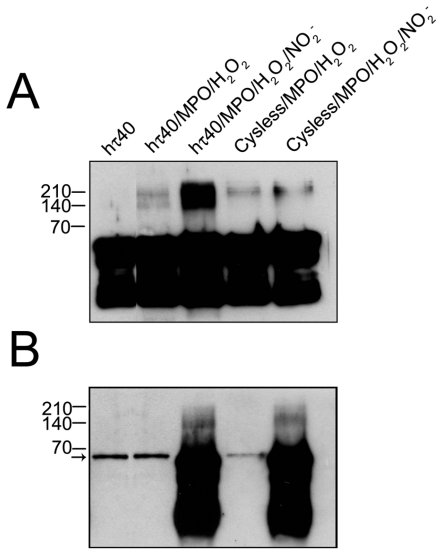

FIGURE 2: Oxidative conditions alone induce the SDS-resistant oligomerization of hτ40. Wild-type hτ40 or hτ40 doubly mutated at both cysteine residues ($^{C}291^{A}/^{C}322^{A}$, termed Cysless) was treated with MPO and H_2O_2 (oxidative conditions) or MPO, H_2O_2, and $NaNO_2$ (oxidative and nitrative conditions). Untreated hτ40 was included as a negative control (lane 1). Proteins were fractionated by SDS−PAGE, transferred onto nitrocellulose membranes, and detected using the antibodies Tau-5 (A) and 3-NT (B). The band migrating at 69 kDa (B, arrow) can be attributed to cross-reactivity of the 3-NT antibody with unmodified hτ40. Fifty (A) and one hundred (B) nanograms of protein were loaded per well. Results are representative of four independent experiments.

cysteine modification contributes to wild-type hτ40 aggregation. As expected, MPO-catalyzed nitration occurs only in the presence of NO_2^- (Figure 2B). Oxidation and/or nitration of hτ40 by MPO, however, occurs less efficiently than with $ONOO^-$ given that it required 10−20-fold more protein per lane to reveal oligomeric hτ40 (50 and 100 ng in panels A and B of Figure 2, respectively). Moreover, in addition to detecting these high-molecular mass bands, longer exposure times reveal the cross-reactivity of the primary antibody with unmodified hτ40 (Figure 2B, arrow) and smaller, C-terminal truncation products that copurify with hτ40 during the protein preparation (Figure 2A and 2B, ≤60 kDa; see Experimental Procedures).

hτ40 Oligomers Contain 3,3′-Dityrosine. Given the structural stability of the hτ40 oligomers, we suspected that the coupling mechanism most likely occurred via a covalent bridge. Further, because disulfide bond formation cannot account for this oxidative cross-linking (Figure 1A, lane 7), and because hτ40 lacks tryptophan residues, another potential oxidative target, we hypothesized that 3,3′-DT was responsible for $ONOO^-$-mediated oligomerization. To test this, purified hτ40 oligomers were acid hydrolyzed into their constituent amino acids and separated by reverse-phase HPLC. A peak was observed by HPLC that coeluted with a purified 3,3′-DT standard (t_R = 17.8 min) and also exhibited the fluorescent signature of 3,3′-DT (λ_{ex} = 283 nm, λ_{em} = 410 nm) (Figure 3A, top and bottom, respectively). Consistent with the mass of 3,3′-DT, the ESI-MS spectrum of this peak shows a molecular ion $(M + H)^+$ at *m*/*z* 361 (Figure 3B). Tandem MS/MS analysis of the molecular ion further confirms the identity of 3,3′-DT, demonstrating the loss of NH_3 and CO_2H groups at *m*/*z* 344 and 315, respectively ([M

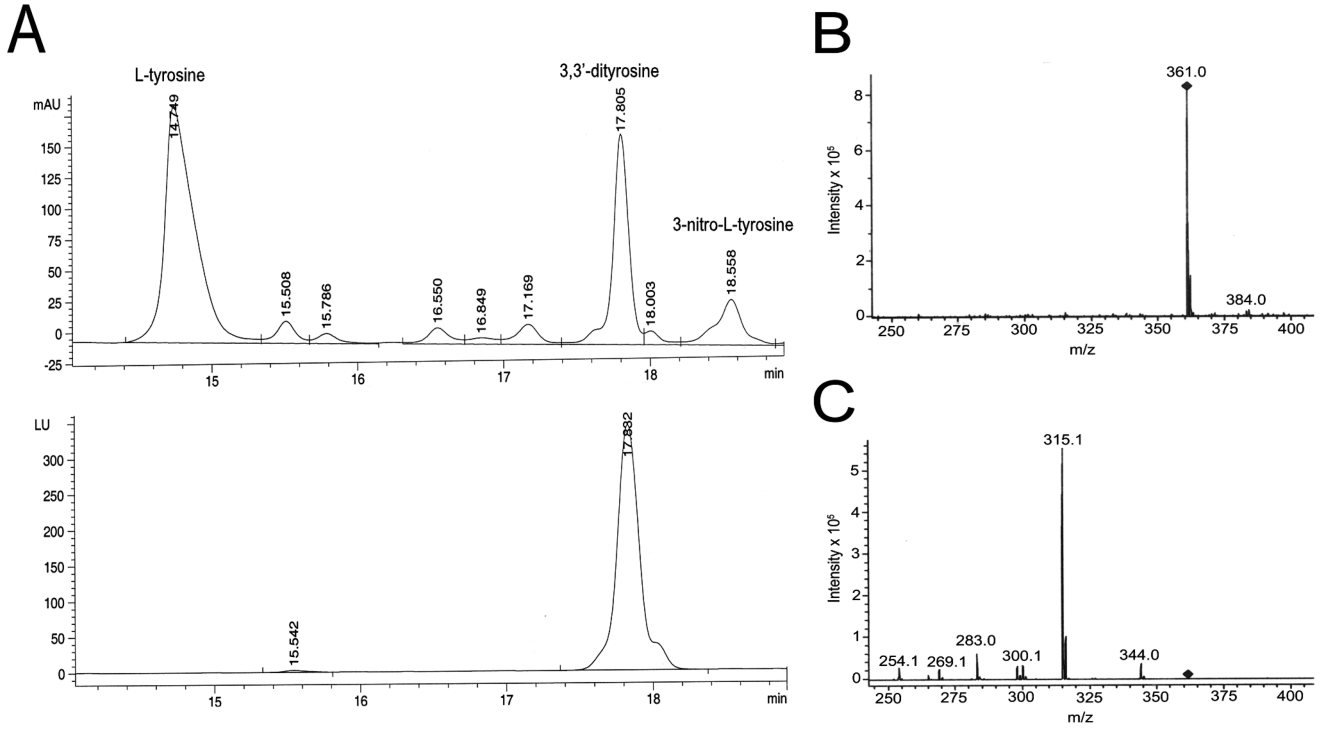

FIGURE 3: hτ40 oligomers are oxidatively cross-linked via 3,3′-dityrosine (3,3′-DT). High-molecular mass hτ40 oligomers were enriched by size-exclusion chromatography and hydrolyzed into their constituent amino acids. (A) Reverse-phase HPLC analysis of hydrolysates using ultraviolet (215 nm; top panel) and fluorescent detection (λ_{ex} = 283 nm, λ_{em} = 410 nm; bottom panel). (B) ESI-MS spectrum of the fluorescent peak from panel A that coelutes with a synthetic 3,3′-DT standard ($t_R \sim 17.8$ min). (C) Tandem MS/MS scan of the molecular ion $(M + H)^+$ at *m*/*z* 361 from panel B.

$+ H]^+$) (Figure 3C). In addition, consistent with our results showing nitration of higher-order oligomers (Figure 1C), a peak was observed by HPLC that coeluted with a 3-nitro-L-tyrosine standard and exhibited the mass ($[M + H]^+$ at *m*/*z* 227) and fragmentation properties of 3-NT (data not shown). Taken together, these data suggest that 3,3-DT promotes and/or stabilizes hτ40 aggregation via Tyr bridging.

Nitration of hτ40 by ONOO⁻ Exhibits Hierarchical Site Specificity. Protein nitration occurs with biological selectivity and can profoundly affect protein folding and function (*33*−*38*). Therefore, as a first step in delineating the structural consequences of τ nitration, we identified the Tyr residues targeted for nitration. To this end, hτ40 monomers were treated with either $ONOO^-$ or degraded $ONOO^-$, trypsinized, and analyzed by MALDI-TOF MS. Peaks were assigned to only those tryptic peptides containing Tyr residues (Figure 4A). Treatment of hτ40 with a 100-fold molar excess of $ONOO^-$ prompts the attenuation of peaks harboring Y18, Y29, and Y197 (Figure 4B). Concomitantly, these same peaks each undergo a mass shift of ∼45 units, corresponding to the addition of a single NO_2 group (Figure 4C−E). Each nitrated peptide then sequentially loses two oxygen atoms (*m*/*z* −16.0 each) to yield characteristic decomposition products (*39*, *40*). Mass analysis of hτ40 lacking the six-His affinity tag demonstrates that the tag has no effect on site-specific hτ40 nitration (data not shown).

Nitration of the tryptic peptides containing Y310 and Y394 was never observed by MALDI. However, these peptides generated low-intensity signals that were occasionally absent in MS scans. Therefore, to verify site-specific nitration of hτ40, mutant proteins were generated to convert four of the five Tyr residues to Phe (Table 1). This approach allowed us to nitrate individual Tyr residues within the context of the full-length protein and to assay site-specific nitration with a 3-NT antibody. Western blot analysis shows that hτ40 nitration by $ONOO^-$ exhibits site selectivity toward residues Y18 and Y29 (Figure 5B). Longer exposure times reveal that Y18, Y29, and to a lesser extent Y197 and Y394 are substrates for $ONOO^-$-mediated nitration (Figure 5C). Y18 and Y29 are the only residues modified when hτ40 is exposed to a 50-fold molar excess of $ONOO^-$ (data not shown). In addition, nitrated hτ40 aggregates are observed in the quadruple Y → F mutants only upon extended exposure times. Intriguingly, Y310 appears to be the least susceptible to nitration, and nitration at this site occurs only minimally at a 100-fold molar excess of $ONOO^-$. As expected, the negative control mutant lacking all Tyr residues is not nitrated and does not generate nitrated oligomers upon $ONOO^-$ exposure (Figure 5A,B).

Each Tyr residue can self-oligomerize, as evidenced by the fact that all the quadruple Y → F mutants demonstrate higher-order bands by Western blot (Figure 5A). $ONOO^-$-mediated oligomerization occurs most efficiently in wild-type hτ40, most likely due to the greater number of Tyr residues available for cross-linking. This efficiency is manifest by the near-complete disappearance of monomeric hτ40 following $ONOO^-$ treatment (Figure 5A, lane 1). Furthermore, hτ40 lacking all Tyr residues (designated 5x Y → F) is incapable of aggregation, suggesting that Tyr residues are essential for $ONOO^-$-mediated oligomerization. Curiously, disulfide bonding does not contribute to oxidative cross-linking in the hτ40 mutant lacking Tyr residues. These results differ markedly from those using MPO-catalyzed hτ40 oxidation (Figure 2), whereby disulfide bonding enhances aggregate formation. Therefore, it is possible that specific oxidizing and/or nitrating agents differentially influence Cys

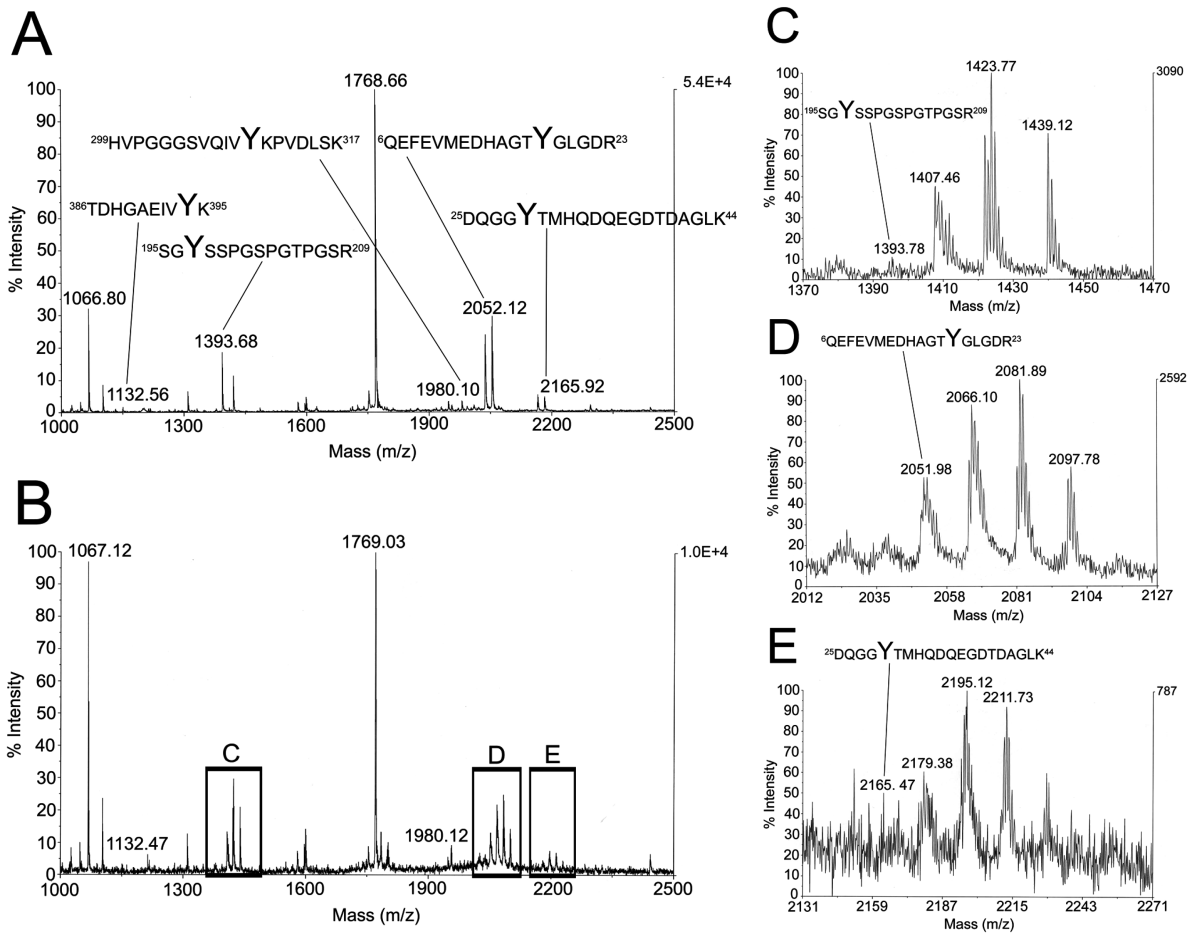

FIGURE 4: Mass mapping of site-specific hτ40 nitration by $ONOO^-$. hτ40 proteins were treated with a 100-fold molar excess of either degraded or active $ONOO^-$, trypsinized overnight, and the peptide fragments were analyzed by MALDI-TOF MS. (A) Peptide mass fingerprinting analysis of nonmodified hτ40 peptides. Peaks have been assigned to only those fragments containing Tyr residues. (B) Mass analysis of nitrated hτ40 peptides. Boxed regions C−E are enlarged in panels C−E. (C) Expanded version of box C from panel B showing select nitration of Y197. (D) Expanded version of box D from panel B showing select nitration of Y18. (E) Expanded version of box E from panel B showing select nitration of Y29. Results are representative of four independent experiments.

cross-linking. Also noteworthy is the fact that the residues most susceptible to nitration (Y18 and Y29, Figure 5B) form 3,3′-DT cross-links most efficiently (Figure 5A). This finding may be attributable to the high accessibility of N-terminal residues to the solvent phase and, therefore, to oxidizing and/or nitrating agents (*41*).

hτ40 Nitration Inhibits in Vitro Polymerization. To determine whether nitration influences hτ40 polymerization, right-angle laser light scattering (LLS) was employed to measure the rate of hτ40 assembly following arachidonic acid induction. This model is useful for kinetic analyses due to the rapid polymerization of full-length hτ40 at near-physiological concentrations (*42*). We have previously shown that light scattering (i_S) is directly proportional to the mass of filamentous hτ40 in suspension (*42*). Nitrated, monomeric hτ40 (see Experimental Procedures) polymerizes to a far lesser extent than wild-type hτ40 (Figure 6A). To examine filament morphology and validate the LLS results, polymerization samples were visualized by EM. While wild-type hτ40 generates abundant filaments (Figure 6B, top), very few filaments are observed in the nitrated hτ40 sample (Figure 6B, bottom). Nitration of hτ40 reduces the average length of filaments per field to 46% [±1.6% standard error of the mean (SEM)] of the hτ40 control, and the average number of filaments to 46% (±3.2% SEM) that of the control. In accordance with the LLS data, this corresponds to a 79% reduction in the average mass of filaments per field (±1.5% SEM).

Pseudophosphorylation of Tyr310 Inhibits in Vitro Polymerization. Numerous post-translational modifications influence τ polymerization (*2*−*6*). To assess whether Tyr phosphorylation also inhibits hτ40 assembly, we generated hτ40 proteins with single Tyr → Glu mutations at each of the five Tyr residues to mimic phosphorylation at these sites (Table 1). LLS analysis of the $^{Y}18^{E}$, $^{Y}29^{E}$, $^{Y}197^{E}$, and $^{Y}394^{E}$ hτ40 mutants, the same residues nitrated by $ONOO^-$ *in vitro*, demonstrates that pseudophosphorylation of these sites does not influence hτ40 assembly relative to the wild-type control (Figure 7A). In fact, only the $^{Y}310^{E}$ modification, the only Tyr residue *not* nitrated by $ONOO^-$ *in vitro*, inhibits hτ40 assembly (Figure 7A). This effect is specific to the chemical nature of the pseudo-phosphate moiety and not to disruption of the Tyr residue, because a $^{Y}310^{F}$ mutant was fully competent to assemble. The reduction in light scattering exhibited by the $^{Y}310^{E}$ mutant was confirmed ultrastructurally by EM (Figure 7B,C). Similar to nitrated hτ40, the $^{Y}310^{E}$ mutant reduced the average length of filaments per field to 47% (±2.1% SEM) of the hτ40 control, and the average number of filaments to 19% (±0.7 SEM) that of the control. There was a 91% reduction in the average mass of filaments per field (±0.1% SEM).

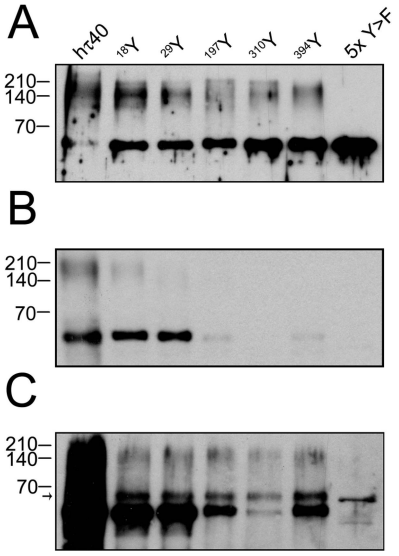

FIGURE 5: Immunodetection of site-specific hτ40 nitration by $ONOO^-$. hτ40 was mutagenized to convert four of the five Tyr residues to Phe (see Table 1) and then treated with a 100-fold molar excess of $ONOO^-$. Proteins were fractionated by SDS−PAGE, transferred onto nitrocellulose membranes, and detected using the antibodies Tau-5 (A) and 3-NT (B and C). Panel C illustrates a longer exposure time of the blot from panel B. Wild-type hτ40 treated with $ONOO^-$ (lane 1) and a $ONOO^-$-treated hτ40 construct lacking all Tyr residues (lane 7) were included as controls. The band migrating at 69 kDa (C, arrow) can be attributed to cross-reactivity of the 3-NT antibody with unmodified hτ40. Five (A) and fifty (B and C) nanograms of protein were loaded per well. Results are representative of four independent experiments.

DISCUSSION

A substantial body of evidence supports the notion that nitrative and oxidative injury contribute to neurodegeneration in AD (*10*−*13*). The levels of 3-NT-modified proteins are significantly elevated in AD brain and cerebrospinal fluid (*43*−*45*). Furthermore, immunohistochemical analyses show that nitrated proteins selectively localize to NFTs in Alzheimer's brain (*10*, *11*). The hippocampus, a region exquisitely vulnerable to NFT formation, demonstrates the greatest change in levels of 3-NT and 3,3′-DT, showing increases of ~8- and 5-fold, respectively, relative to age-matched controls (*19*). More recently, several of the proteinaceous targets of nitration and oxidation have been identified. Using an antibody that recognizes nitrated *τ*, Horiguchi *et al.* (*21*) demonstrate staining of pretangles, tangles, and *τ* inclusions in AD brain. The robust staining of pretangles in early AD cases (Braak and Braak stage I-II) and the diminution of staining in more advanced cases (Braak and Braak stage V-VI) suggest that *τ* nitration may be an early event in AD (*21*). In addition, several reports show that oxidative 3,3′-DT cross-linking promotes the oligomerization of proteins known to aggregate in neurodegenerative disease (*17*, *18*). Although these findings implicate oxidative and nitrative modifications in the self-assembly of disease proteins, the relationship between oxidation/nitration and *τ* polymerization has heretofore remained elusive.

$ONOO^-$ Promotes the SDS-Resistant Oligomerization of hτ40. In this report, we examine the effects of $ONOO^-$-mediated nitration and oxidation on *τ* polymerization *in vitro*. Our data demonstrate that (1) hτ40 is a substrate for nitration and oxidative 3,3′-DT cross-linking by $ONOO^-$, (2) Tyr

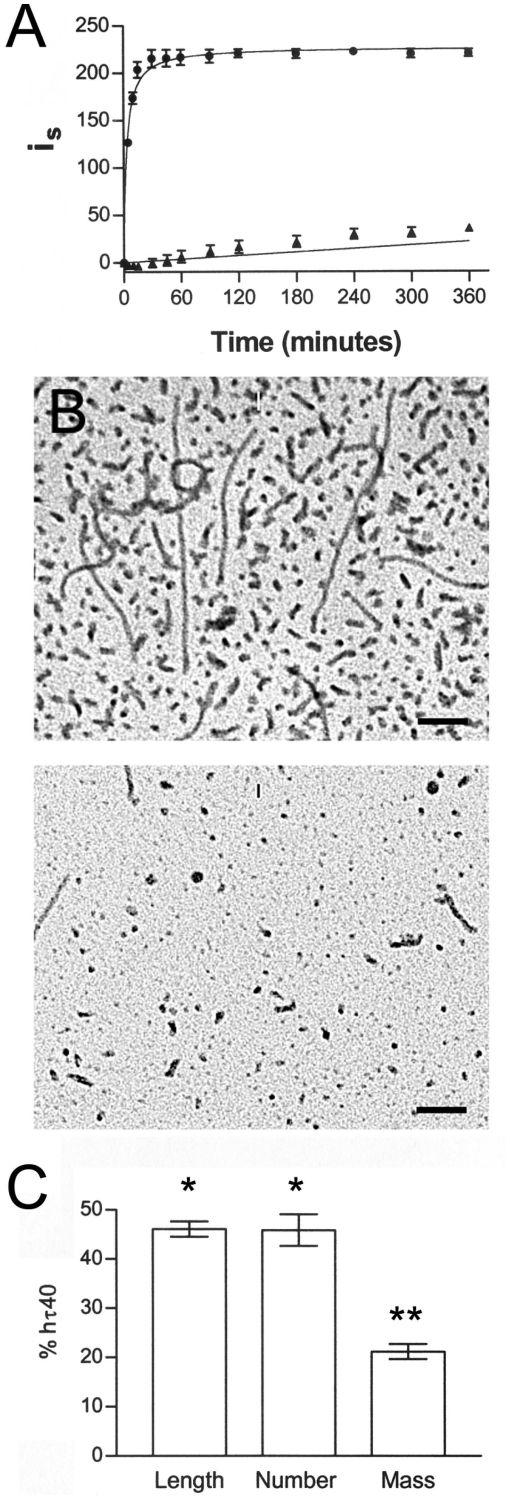

FIGURE 6: Nitration of hτ40 by $ONOO^-$ inhibits *in vitro* polymerization. Right-angle laser light scattering was performed to measure the rate of hτ40 assembly following arachidonic acid induction. (A) The intensity of scattered light (i_s) is shown as a function of induction time for nonmodified (●) and nitrated hτ40 (▲). Data are plotted as the mean ± SEM of four independent measurements. (B) Negative-stain electron micrographs of nonmodified (top) and nitrated (bottom) hτ40 filaments following a 6 h induction period. (C) Quantitative EM measurements from nonmodified and nitrated hτ40 filaments. The average length, number, and mass per field of nitrated hτ40 filaments are expressed relative to nonmodified hτ40 filaments. Results are from four independent experiments, and error bars represent the SEM ($* = p < 0.005$; $** = p < 0.001$). The size bar represents 500 nm.

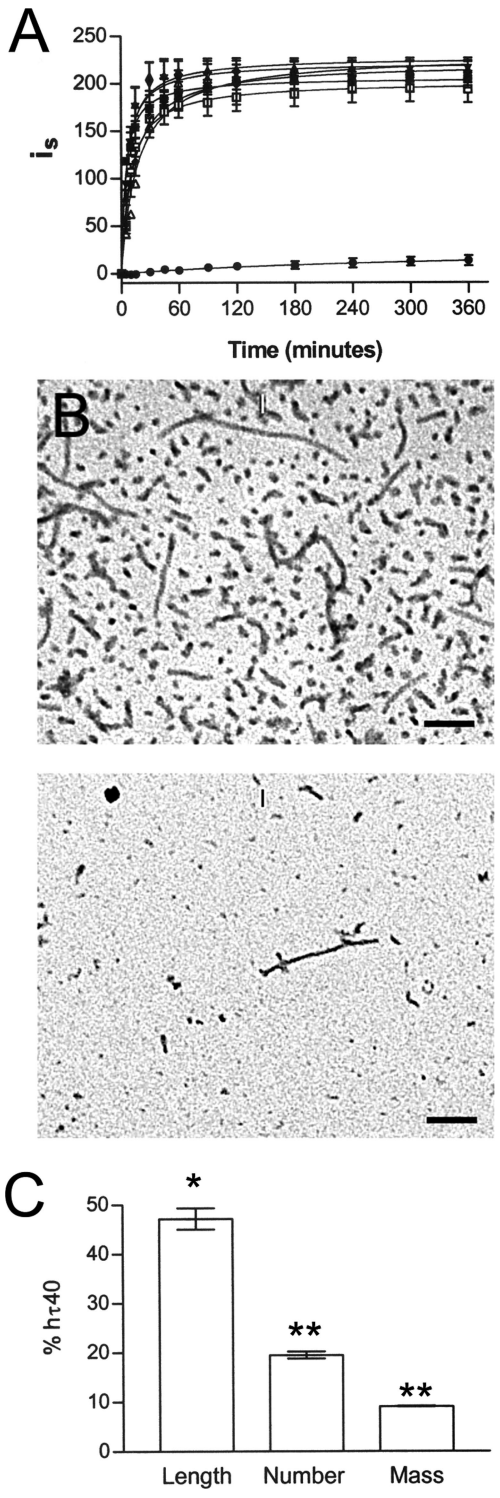

FIGURE 7: Pseudophosphorylation at $^{Y}310^{E}$ inhibits hτ40 polymerization *in vitro*. Right-angle laser light scattering was performed to measure the rate of hτ40 assembly following arachidonic acid induction. (A) The intensity of scattered light (i_s) is shown as a function of induction time for wild-type (■) and mutant [$^{Y}18^{E}$ (▲), $^{Y}29^{E}$ (▼), $^{Y}197^{E}$ (◆), $^{Y}310^{E}$ (●), $^{Y}394^{E}$ (□), and $^{Y}310^{F}$ (△)] hτ40. Data are plotted as the mean ± SEM of four independent measurements. (B) Negative stain electron micrographs of wild-type (top) and $^{Y}310^{E}$ (bottom) hτ40 filaments following a 6 h induction period. (C) Quantitative EM measurements from wild-type and $^{Y}310^{E}$ hτ40 filaments. The average length, number, and mass per field of $^{Y}310^{E}$ hτ40 filaments are expressed relative to nonmodified hτ40 filaments. Results are from four independent experiments, and error bars represent the SEM (* = $p < 0.005$; ** = $p < 0.0005$). The size bar represents 500 nm.

residues are essential for $ONOO^-$-mediated oligomerization, (3) site-specific nitration of Y18, Y29, and to a lesser degree Y197 and Y394 inhibits hτ40 polymerization, and (4) pseudophosphorylation at these same residues does not recapitulate the inhibitory effect on hτ40 assembly. The ability of hτ40 to form thermally stable, SDS-insoluble oligomers through 3,3′-DT bridging has important implications for τ metabolism and Alzheimer's pathogenesis. Perhaps most importantly, the 3,3′-DT bond facilitates conversion of monomeric hτ40 into higher-molecular mass oligomers. This covalent link would enhance the structural integrity of polymeric τ and confer resistance to denaturing and chaotropic agents (*17*, *18*). Unlike the transitory disulfide bonding between adjacent Cys residues, 3,3′-DT bonds are irreversible and highly resistant to proteolytic degradation. In fact, by SDS−PAGE, these oligomers are highly reminiscent of fibrillar τ derived from post-mortem AD brain (*46*, *47*) and may explain how a wild-type protein devoid of secondary structure can form highly insoluble deposits.

One possible mechanism for how 3,3′-DT cross-linking could contribute to AD neurodegeneration is by stabilizing preformed τ filaments. Evidence from *in vivo* animal models demonstrates that a substantial τ filament burden is required for degenerative changes (*48*). This finding suggests that τ filaments *alone* may not be sufficient for cytotoxicity. However, stabilization of τ filaments through 3,3′-DT bridging could reduce their solubility and deter proteolysis, thereby preventing the efficient removal of τ filaments from the neuron. The buildup of filamentous τ protein may subsequently lead to inclusion body formation and neurodegeneration.

Given that the cellular concentration of τ is estimated to be 2−4 μM (*42*) and 3,3′-DT bridging of hτ40 occurs at a 5-fold molar excess of $ONOO^-$ *in vitro* (Figure 1A), we estimate that a $ONOO^-$ concentration of only 10−20 μM would be necessary to oligomerize τ *in vivo*. Under conditions of oxidative stress, which occurs during AD-associated inflammation, this concentration of $ONOO^-$ is highly plausible (*27*, *33*) and could convert soluble τ into insoluble polymers or stabilize pre-existing polymers. This cross-linking event may, therefore, provide a putative link between neuroinflammation and pathological protein deposition.

Structural and Functional Implications of Site-Specific Nitration. Only a select number of proteins are modified by nitration *in vivo* (*27*, *33*). Importantly, of those proteins subject to nitration, only specific Tyr residues are modified (*49*−*53*). Based upon the factors that influence nitration *in vitro*, it is not surprising that the N-terminal Tyr residues of τ (Y18 and Y29) are primary substrates for nitration. The N-terminus of τ lacks any demonstrable tendency to form secondary structure (*41*) and projects away from the microtubule (MT) surface when τ is bound to MTs (*54*). Due to this paucity of structure and high level of exposure to the solvent phase, these residues are highly accessible to modification. The N-terminal Tyr residues also lie within a carboxylic acid-rich environment, are adjacent to several turn-inducing residues, and are removed from nearby Cys residues that are alternative targets for oxidation and can provide steric hindrance by disulfide bridging (*55*). Significantly, Y310 and Y394 both lie in the predicted β-sheet regions of τ (*42*), and this factor might preclude nitration at these sites.

Our observation that 3-NT modification is unfavorable at Y310 suggests that nitration inhibits hτ40 assembly in a manner distinct from pseudophosphorylation. Y310 resides within a hexapeptide motif (^{306}VQIVYK^{311}) known to be essential for *in vitro* τ assembly (*9*). Consistent with our data, pseudophosphorylation at Y310 may prevent the stacking interaction necessary for τ polymerization (*56*), thereby inhibiting τ filament formation. Moreover, previous work from our laboratory has shown that τ undergoes a change in conformation whereby the N-terminus folds back upon the third MT binding repeat. This event coincides with early filamentous changes in τ and is detected by the conformation-sensitive antibody Alz-50 (*22*, *57*). It has also been proposed that the Alz-50 interaction between the negatively charged N-terminus of τ and the positively charged MT binding repeat may be electrostatic in nature (*42*). If so, nitration at Y18 and/or Y29 may sterically hinder the Alz-50 conformation, thereby preventing τ polymerization. Alternatively, Y197 lies within a proline-rich "hinge" region that imparts flexibility to the τ molecule that is necessary for the Alz-50 conformation to occur (*42*). Nitration at Y197 may reduce this flexibility, straighten the τ backbone, and preclude the Alz-50 conformation. Spontaneous formation of the Alz-50 conformation may also explain the site-specific and hierarchical nitration of τ observed *in vitro*. It is entirely conceivable that τ can assume a solution conformation (i.e., Alz-50 conformation) that does not involve a change in secondary structure detectable by circular dichroism spectroscopy (*22*). Assumption of the Alz-50 conformation could then account for the preferential nitration of the N-terminal residues Y18 and Y29.

We clearly show that nitration and pseudophosphorylation of specific Tyr residues can differentially affect τ polymerization *in vitro*. One potential *in vivo* correlate to these findings is that oxidizing agents and kinases may compete to fill these same sites. Recent work shows that Y18 of τ can be phosphorylated by the src family tyrosine kinase, fyn, and that fyn is upregulated in a subset of AD neurons (*58*, *59*). Moreover, phosphorylation of Y18 occurs in paired helical filament preparations extracted from AD brain (*58*). This finding is consistent with our results showing that pseudophosphorylation at Y18 is permissive to hτ40 assembly. Our data also show that nitration of Y18 may serve to prevent τ polymerization, given that Y18 and Y29 are the primary substrates of $ONOO^-$ and that nitration inhibits hτ40 assembly. Accordingly, competition to fill the Y18 site may shift the equilibrium of τ molecules toward monomer (nitration of Y18) or polymer (phosphorylation of Y18). Because no known "nitrases" have been isolated *in vivo*, however, nitration may exert a more lasting effect on τ polymerization (*33*).

Our finding that $ONOO^-$-mediated nitration inhibits τ polymerization suggests that this pathway may protect against pathological protein deposition. For example, upon Aβ peptide stimulation, microglia increase production of $O_2^{\bullet -}$ (*60*−*62*) and upregulate the inducible form of nitric oxide synthase (iNOS) to yield high levels of $NO^\bullet$ (*63*, *64*). Induction of $NO^\bullet$ and $O_2^{\bullet -}$ results in $ONOO^-$ generation with subsequent protein nitration. Accordingly, in Alzheimer's brain, microgliosis adjacent to neurons containing intracellular τ fibrils may serve to prevent τ polymerization and, subsequently, NFT formation. Chronic, unregulated production of $ONOO^-$ by reactive glia, however, may negate the beneficial effects of nitration by stabilizing τ aggregates through oxidative 3,3′-DT cross-linking. However, our results cannot exclude the possibility that small aggregates produced from nitrated τ monomers might even be more cytotoxic than the filaments assembled from the wild-type τ protein (*65*).

Collectively, our data suggest that $ONOO^-$ exerts antagonistic effects on τ polymerization based upon its dichotomous nitrative and oxidative roles. To our knowledge, this is the first report to demonstrate τ cross-linking through 3,3′-DT and to show that site-specific nitration impacts τ polymerization. Additional studies will be required to determine the significance of site-specific nitration and oxidative 3,3′-DT bridging *in vivo*. Nonetheless, these findings contribute to a rapidly expanding body of knowledge illustrating how post-translational events influence τ self-assembly in Alzheimer's brain.

ACKNOWLEDGMENT

We acknowledge Drs. Thomas J. Lukas, D. Martin Watterson, and Teepu Siddique of Northwestern University for invaluable advice and technical assistance with MALDI-TOF and ESI mass spectrometry. We also thank Drs. Virginia M.-Y. Lee, Harry Ischiropoulos, and Jerome J. Garcia (University of Pennsylvania, Philadelphia, PA) for technical advice regarding 3,3′-dityrosine and Dr. T. Chris Gamblin (University of Kansas, Lawrence, KS) for critical reading of the manuscript. MALDI-TOF MS and ESI-MS were performed at the Analytical Services Laboratory of Northwestern University. HPLC measurements were taken at the Keck Biophysics Facility of Northwestern University.

REFERENCES

1. Schweers, O., Schonbrunn-Hanebeck, E., Marx, A., and Mandelkow, E. (1994) Structural studies of tau protein and Alzheimer paired helical filaments show no evidence for β-structure, *J. Biol. Chem. 269*, 24290−24297.
2. Grundke-Iqbal, I., Iqbal, K., Tung, Y. C., Quinlan, M., Wisniewski, H. M., and Binder, L. I. (1986) Abnormal phosphorylation of the microtubule-associated protein tau (tau) in Alzheimer cytoskeletal pathology, *Proc. Natl. Acad. Sci. U.S.A. 83*, 4913−4917.
3. Alonso, A. C., Grundke-Iqbal, I., and Iqbal, K. (1996) Alzheimer's disease hyperphosphorylated tau sequesters normal tau into tangles of filaments and disassembles microtubules, *Nat. Med. 2*, 783−787.
4. Gamblin, T. C., Chen, F., Zambrano, A., Abraha, A., Lagalwar, S., Guillozet, A. L., Lu, M., Fu, Y., Garcia-Sierra, F., LaPointe, N., Miller, R., Berry, R. W., Binder, L. I., and Cryns, V. L. (2003) Caspase cleavage of tau: Linking amyloid and neurofibrillary tangles in Alzheimer's disease, *Proc. Natl. Acad. Sci. U.S.A. 100*, 10032−1007.
5. Garcia-Sierra, F., Ghoshal, N., Quinn, B., Berry, R. W., and Binder, L. I. (2003) Conformational changes and truncation of tau protein during tangle evolution in Alzheimer's disease, *J. Alzheimer's Dis. 5*, 65−77.
6. Ghoshal, N., Garcia-Sierra, F., Wuu, J., Leurgans, S., Bennett, D. A., Berry, R. W., and Binder, L. I. (2002) Tau conformational changes correspond to impairments of episodic memory in mild cognitive impairment and Alzheimer's disease, *Exp. Neurol. 177*, 475−493.
7. von Bergen, M., Barghorn, S., Li, L., Marx, A., Biernat, J., Mandelkow, E. M., and Mandelkow, E. (2001) Mutations of tau protein in frontotemporal dementia promote aggregation of paired helical filaments by enhancing local β-structure, *J. Biol. Chem. 276*, 48165−48174.
8. Giannetti, A. M., Lindwall, G., Chau, M. F., Radeke, M. J., Feinstein, S. C., and Kohlstaedt, L. A. (2000) Fibers of tau fragments, but not full length tau, exhibit a cross β-structure:

Implications for the formation of paired helical filaments, *Protein Sci. 9*, 2427−2435.
9. von Bergen, M., Friedhoff, P., Biernat, J., Heberle, J., Mandelkow, E. M., and Mandelkow, E. (2000) Assembly of tau protein into Alzheimer paired helical filaments depends on a local sequence motif ((306)VQIVYK(311)) forming β structure, *Proc. Natl. Acad. Sci. U.S.A. 97*, 5129−5134.
10. Good, P. F., Werner, P., Hsu, A., Olanow, C. W., and Perl, D. P. (1996) Evidence of neuronal oxidative damage in Alzheimer's disease, *Am. J. Pathol. 149*, 21−28.
11. Smith, M. A., Richey Harris, P. L., Sayre, L. M., Beckman, J. S., and Perry, G. (1997) Widespread peroxynitrite-mediated damage in Alzheimer's disease, *J. Neurosci. 17*, 2653−2657.
12. Markesbery, W. R., and Carney, J. M. (1999) Oxidative alterations in Alzheimer's disease, *Brain Pathol. 9*, 133−146.
13. Multhaup, G., Ruppert, T., Schlicksupp, A., Hesse, L., Beher, D., Masters, C. L., and Beyreuther, K. (1997) Reactive oxygen species and Alzheimer's disease, *Biochem. Pharmacol. 54*, 533−539.
14. Ischiropoulos, H., Zhu, L., Chen, J., Tsai, M., Martin, J. C., Smith, C. D., and Beckman, J. S. (1992) Peroxynitrite-mediated tyrosine nitration catalyzed by superoxide dismutase, *Arch. Biochem. Biophys. 298*, 431−437.
15. Beckman, J. S. (1996) Oxidative damage and tyrosine nitration from peroxynitrite, *Chem. Res. Toxicol. 9*, 836−844.
16. Beckman, J. S., and Koppenol, W. H. (1996) Nitric oxide, superoxide, and peroxynitrite: The good, the bad, and ugly, *Am. J. Physiol. 271*, C1424−C1437.
17. Souza, J. M., Giasson, B. I., Chen, Q., Lee, V. M., and Ischiropoulos, H. (2000) Dityrosine cross-linking promotes formation of stable α-synuclein polymers. Implication of nitrative and oxidative stress in the pathogenesis of neurodegenerative synucleinopathies, *J. Biol. Chem. 275*, 18344−18349.
18. Atwood, C. S., Perry, G., Zeng, H., Kato, Y., Jones, W. D., Ling, K. Q., Huang, X., Moir, R. D., Wang, D., Sayre, L. M., Smith, M. A., Chen, S. G., and Bush, A. I. (2004) Copper mediates dityrosine cross-linking of Alzheimer's amyloid-β, *Biochemistry 43*, 560−568.
19. Hensley, K., Maidt, M. L., Yu, Z., Sang, H., Markesbery, W. R., and Floyd, R. A. (1998) Electrochemical analysis of protein nitrotyrosine and dityrosine in the Alzheimer brain indicates region-specific accumulation, *J. Neurosci. 18*, 8126−8132.
20. Giasson, B. I., Duda, J. E., Murray, I. V., Chen, Q., Souza, J. M., Hurtig, H. I., Ischiropoulos, H., Trojanowski, J. Q., and Lee, V. M. (2000) Oxidative damage linked to neurodegeneration by selective α-synuclein nitration in synucleinopathy lesions, *Science 290*, 985−989.
21. Horiguchi, T., Uryu, K., Giasson, B. I., Ischiropoulos, H., LightFoot, R., Bellmann, C., Richter-Landsberg, C., Lee, V. M., and Trojanowski, J. Q. (2003) Nitration of tau protein is linked to neurodegeneration in tauopathies, *Am. J. Pathol. 163*, 1021−1031.
22. Carmel, G., Mager, E. M., Binder, L. I., and Kuret, J. (1996) The structural basis of monoclonal antibody Alz50's selectivity for Alzheimer's disease pathology, *J. Biol. Chem. 271*, 32789−32795.
23. Abraha, A., Ghoshal, N., Gamblin, T. C., Cryns, V., Berry, R. W., Kuret, J., and Binder, L. I. (2000) C-Terminal inhibition of tau assembly in vitro and in Alzheimer's disease, *J. Cell Sci. 113* (Part 21), 3737−3745.
24. Lowry, O. H., Rosebrough, N. J., Farr, A. L., and Randall, R. J. (1951) Protein measurement with the Folin phenol reagent, *J. Biol. Chem. 193*, 265−275.
25. Beckman, J. S., Chen, J., Ischiropoulos, H., and Crow, J. P. (1994) Oxidative chemistry of peroxynitrite, *Methods Enzymol. 233*, 229−240.
26. Uppu, R. M., Squadrito, G. L., Cueto, R., and Pryor, W. A. (1996) Selecting the most appropriate synthesis of peroxynitrite, *Methods Enzymol. 269*, 285−296.
27. Souza, J. M., Daikhin, E., Yudkoff, M., Raman, C. S., and Ischiropoulos, H. (1999) Factors determining the selectivity of protein tyrosine nitration, *Arch. Biochem. Biophys. 371*, 169−178.
28. Ischiropoulos, H., and al-Mehdi, A. B. (1995) Peroxynitrite-mediated oxidative protein modifications, *FEBS Lett. 364*, 279−282.
29. White, C. R., Patel, R. P., and Darley-Usmar, V. (1999) Nitric oxide donor generation from reactions of peroxynitrite, *Methods Enzymol. 301*, 288−298.
30. Viera, L., Ye, Y. Z., Estevez, A. G., and Beckman, J. S. (1999) Immunohistochemical methods to detect nitrotyrosine, *Methods Enzymol. 301*, 373−381.
31. Gamblin, T. C., King, M. E., Kuret, J., Berry, R. W., and Binder, L. I. (2000) Oxidative regulation of fatty acid-induced tau polymerization, *Biochemistry 39*, 14203−14210.
32. King, M. E., Gamblin, T. C., Kuret, J., and Binder, L. I. (2000) Differential assembly of human tau isoforms in the presence of arachidonic acid, *J. Neurochem. 74*, 1749−1757.
33. Ischiropoulos, H. (2003) Biological selectivity and functional aspects of protein tyrosine nitration, *Biochem. Biophys. Res. Commun. 305*, 776−783.
34. Greenacre, S. A., and Ischiropoulos, H. (2001) Tyrosine nitration: Localisation, quantification, consequences for protein function and signal transduction, *Free Radical Res. 34*, 541−581.
35. MacMillan-Crow, L. A., Crow, J. P., and Thompson, J. A. (1998) Peroxynitrite-mediated inactivation of manganese superoxide dismutase involves nitration and oxidation of critical tyrosine residues, *Biochemistry 37*, 1613−1622.
36. Takakura, K., Beckman, J. S., MacMillan-Crow, L. A., and Crow, J. P. (1999) Rapid and irreversible inactivation of protein tyrosine phosphatases PTP1B, CD45, and LAR by peroxynitrite, *Arch. Biochem. Biophys. 369*, 197−207.
37. Roberts, E. S., Lin, H., Crowley, J. R., Vuletich, J. L., Osawa, Y., and Hollenberg, P. F. (1998) Peroxynitrite-mediated nitration of tyrosine and inactivation of the catalytic activity of cytochrome P450 2B1, *Chem. Res. Toxicol. 11*, 1067−1074.
38. Ara, J., Przedborski, S., Naini, A. B., Jackson-Lewis, V., Trifiletti, R. R., Horwitz, J., and Ischiropoulos, H. (1998) Inactivation of tyrosine hydroxylase by nitration following exposure to peroxynitrite and 1-methyl-4-phenyl-1,2,3,6-tetrahydropyridine (MPTP), *Proc. Natl. Acad. Sci. U.S.A. 95*, 7659−7663.
39. Sarver, A., Scheffler, N. K., Shetlar, M. D., and Gibson, B. W. (2001) Analysis of peptides and proteins containing nitrotyrosine by matrix-assisted laser desorption/ionization mass spectrometry, *J. Am. Soc. Mass Spectrom. 12*, 439−448.
40. Borges, C. R., Kuhn, D. M., and Watson, J. T. (2003) Mass mapping sites of nitration in tyrosine hydroxylase: Random vs selective nitration of three tyrosine residues, *Chem. Res. Toxicol. 16*, 536−540.
41. Gamblin, T. C., Berry, R. W., and Binder, L. I. (2003) Tau polymerization: Role of the amino terminus, *Biochemistry 42*, 2252−2257.
42. Gamblin, T. C., Berry, R. W., and Binder, L. I. (2003) Modeling tau polymerization in vitro: A review and synthesis, *Biochemistry 42*, 15009−15017.
43. Williamson, K. S., Gabbita, S. P., Mou, S., West, M., Pye, Q. N., Markesbery, W. R., Cooney, R. V., Grammas, P., Reimann-Philipp, U., Floyd, R. A., and Hensley, K. (2002) The nitration product 5-nitro-γ-tocopherol is increased in the Alzheimer brain, *Nitric Oxide 6*, 221−227.
44. Castegna, A., Thongboonkerd, V., Klein, J. B., Lynn, B., Markesbery, W. R., and Butterfield, D. A. (2003) Proteomic identification of nitrated proteins in Alzheimer's disease brain, *J. Neurochem. 85*, 1394−1401.
45. Tohgi, H., Abe, T., Yamazaki, K., Murata, T., Ishizaki, E., and Isobe, C. (1999) Alterations of 3-nitrotyrosine concentration in the cerebrospinal fluid during aging and in patients with Alzheimer's disease, *Neurosci. Lett. 269*, 52−54.
46. Brion, J. P., Hanger, D. P., Couck, A. M., and Anderton, B. H. (1991) A68 proteins in Alzheimer's disease are composed of several tau isoforms in a phosphorylated state which affects their electrophoretic mobilities, *Biochem. J. 279* (Part 3), 831−836.
47. Lee, V. M., Goedert, M., and Trojanowski, J. Q. (2001) Neurodegenerative tauopathies, *Annu. Rev. Neurosci. 24*, 1121−1159.
48. Hall, G. F., Yao, J., and Lee, G. (1997) Human tau becomes phosphorylated and forms filamentous deposits when overexpressed in lamprey central neurons in situ, *Proc. Natl. Acad. Sci. U.S.A. 94*, 4733−4738.
49. Berlett, B. S., Friguet, B., Yim, M. B., Chock, P. B., and Stadtman, E. R. (1996) Peroxynitrite-mediated nitration of tyrosine residues in *Escherichia coli* glutamine synthetase mimics adenylylation: Relevance to signal transduction, *Proc. Natl. Acad. Sci. U.S.A. 93*, 1776−1780.
50. Blanchard-Fillion, B., Souza, J. M., Friel, T., Jiang, G. C., Vrana, K., Sharov, V., Barron, L., Schoneich, C., Quijano, C., Alvarez, B., Radi, R., Przedborski, S., Fernando, G. S., Horwitz, J., and Ischiropoulos, H. (2001) Nitration and inactivation of tyrosine hydroxylase by peroxynitrite, *J. Biol. Chem. 276*, 46017−46023.

51. Zou, M. H., Leist, M., and Ullrich, V. (1999) Selective nitration of prostacyclin synthase and defective vasorelaxation in atherosclerotic bovine coronary arteries, *Am. J. Pathol. 154*, 1359−1365.
52. Viner, R. I., Ferrington, D. A., Williams, T. D., Bigelow, D. J., and Schoneich, C. (1999) Protein modification during biological aging: Selective tyrosine nitration of the SERCA2a isoform of the sarcoplasmic reticulum Ca^{2+}-ATPase in skeletal muscle, *Biochem. J. 340* (Part 3), 657−669.
53. Yamakura, F., Taka, H., Fujimura, T., and Murayama, K. (1998) Inactivation of human manganese-superoxide dismutase by peroxynitrite is caused by exclusive nitration of tyrosine 34 to 3-nitrotyrosine, *J. Biol. Chem. 273*, 14085−14089.
54. Buee, L., Bussiere, T., Buee-Scherrer, V., Delacourte, A., and Hof, P. R. (2000) Tau protein isoforms, phosphorylation and role in neurodegenerative disorders, *Brain Res. Brain Res. Rev. 33*, 95−130.
55. Alvarez, B., Ferrer-Sueta, G., Freeman, B. A., and Radi, R. (1999) Kinetics of peroxynitrite reaction with amino acids and human serum albumin, *J. Biol. Chem. 274*, 842−848.
56. Margittai, M., and Langen, R. (2004) Template-assisted filament growth by parallel stacking of tau, *Proc. Natl. Acad. Sci. U.S.A. 101*, 10278−10283.
57. Hyman, B. T., Van Hoesen, G. W., Wolozin, B. L., Davies, P., Kromer, L. J., and Damasio, A. R. (1988) Alz-50 antibody recognizes Alzheimer-related neuronal changes, *Ann. Neurol. 23*, 371−379.
58. Lee, G., Thangavel, R., Sharma, V. M., Litersky, J. M., Bhaskar, K., Fang, S. M., Do, L. H., Andreadis, A., Van Hoesen, G., and Ksiezak-Reding, H. (2004) Phosphorylation of tau by fyn: Implications for Alzheimer's disease, *J. Neurosci. 24*, 2304−2312.
59. Shirazi, S. K., and Wood, J. G. (1993) The protein tyrosine kinase, fyn, in Alzheimer's disease pathology, *NeuroReport 4*, 435−437.
60. McDonald, D. R., Brunden, K. R., and Landreth, G. E. (1997) Amyloid fibrils activate tyrosine kinase-dependent signaling and superoxide production in microglia, *J. Neurosci. 17*, 2284−2294.
61. Colton, C. A., and Gilbert, D. L. (1987) Production of superoxide anions by a CNS macrophage, the microglia, *FEBS Lett. 223*, 284−288.
62. Klegeris, A., and McGeer, P. L. (1994) Rat brain microglia and peritoneal macrophages show similar responses to respiratory burst stimulants, *J. Neuroimmunol. 53*, 83−90.
63. Goodwin, J. L., Uemura, E., and Cunnick, J. E. (1995) Microglial release of nitric oxide by the synergistic action of β-amyloid and IFN-γ, *Brain Res. 692*, 207−214.
64. Ii, M., Sunamoto, M., Ohnishi, K., and Ichimori, Y. (1996) β-Amyloid protein-dependent nitric oxide production from microglial cells and neurotoxicity, *Brain Res. 720*, 93−100.
65. Caughey, B., and Lansbury, P. T. (2003) Protofibrils, pores, fibrils, and neurodegeneration: Separating the responsible protein aggregates from the innocent bystanders, *Annu. Rev. Neurosci. 26*, 267−298.

BI047982V